A Compartmental Model for Biokinetics and Dosimetry of ^{18}F-Choline in Prostate Cancer Patients

Augusto Giussani[1], Tilman Janzen[1], Helena Uusijärvi-Lizana[2], Federico Tavola[3], Maria Zankl[1], Marie Sydoff[2], Anders Bjartell[4], Sigrid Leide-Svegborn[2], Marcus Söderberg[2], Sören Mattsson[2], Christoph Hoeschen[1], and Marie-Claire Cantone[3]

[1]Helmholtz Zentrum München, German Research Center for Environmental Health, Research Unit Medical Radiation Physics and Diagnostics, Neuherberg, Germany; [2]Medical Radiation Physics, Lund University and Skåne University Hospital Malmö, Malmö, Sweden; [3]Dipartimento di Fisica, Università degli Studi di Milano and INFN, Milano, Italy; and [4]Department of Urology, Skåne University Hospital Malmö, and Lund University, Malmö, Sweden

PET with ^{18}F-choline (^{18}F-FCH) is used in the diagnosis of prostate cancer and its recurrences. In this work, biodistribution data from a recent study conducted at Skåne University Hospital Malmö were used for the development of a biokinetic and dosimetric model. **Methods:** The biodistribution of ^{18}F-FCH was followed for 10 patients using PET up to 4 h after administration. Activity concentrations in blood and urine samples were also determined. A compartmental model structure was developed, and values of the model parameters were obtained for each single patient and for a reference patient using a population kinetic approach. Radiation doses to the organs were determined using computational (voxel) phantoms for the determination of the S factors. **Results:** The model structure consists of a central exchange compartment (blood), 2 compartments each for the liver and kidneys, 1 for spleen, 1 for urinary bladder, and 1 generic compartment accounting for the remaining material. The model can successfully describe the individual patients' data. The parameters showing the greatest interindividual variations are the blood volume (the clearance process is rapid, and early blood data are not available for several patients) and the transfer out from liver (the physical half-life of ^{18}F is too short to follow this long-term process with the necessary accuracy). The organs receiving the highest doses are the kidneys (reference patient, 0.079 mGy/MBq; individual values, 0.033–0.105 mGy/MBq) and the liver (reference patient, 0.062 mGy/MBq; individual values, 0.036–0.082 mGy/MBq). The dose to the urinary bladder wall of the reference patient varies between 0.017 and 0.030 mGy/MBq, depending on the assumptions on bladder voiding. **Conclusion:** The model gives a satisfactory description of the biodistribution of ^{18}F-FCH and realistic estimates of the radiation dose received by the patients.

Key Words: ^{18}F-choline; PET; prostate carcinoma; biokinetics; dosimetry

Choline uptake is increased in cancerous tissues because the high metabolic rates of tumor cells require choline for the synthesis of phospholipids. For example, choline kinase is overexpressed in prostate cancer cells (1,2), thus making choline a suitable indicator for early and differential diagnosis of prostate cancer.

PET with radiolabeled choline is therefore used for diagnosis of malignant and recurrent tumors and of metastases in prostate cancer patients (3–7). A correct evaluation of the patient dose and the optimization of the imaging protocols imply knowledge of the biodistribution and kinetics of the administered compounds. Recently, the biokinetics of ^{18}F-choline (^{18}F-FCH) in 4 prostate cancer patients were investigated in a study conducted in the frame of the European Collaborative project MADEIRA (Minimizing Activity and Dose with Enhanced Image quality by Radiopharmaceutical Administrations (8–9)). Six new patients have now been included in the study. In these investigations, biodistribution and excretion data were collected for up to 4 h after injection of the radiopharmaceutical. Previous human studies with ^{11}C- or ^{18}F-choline were limited up to 1 h after administration (3–7,10).

The aim of this work was to develop a compartmental model for ^{18}F-choline using the patients' data collected in the MADEIRA study. The study presented here represents 1 of the 2 different modeling approaches independently pursued within the project (11). Preliminary results on a smaller set of patients were presented at the 2010 meeting of the International Society for Optics and Photonics SPIE (12).

MATERIALS AND METHODS

Biokinetic Studies

Patient measurements were performed at the Department for Imaging and Functional Medicine of the Skåne University Hospital in Malmö according to the protocol approved by the Regional Ethical Vetting Board at Lund University. ^{18}F-FCH was synthesized using a TRACERlab MX module (GE Healthcare) and reagent kits (ABX GmbH) at the cyclotron facilities at

Skåne University Hospital in Lund and then delivered to Malmö.

Ten patients (age range, 59–77 y) with a previous history of prostatectomy and raised prostate-specific antigen levels detected during a control check were enrolled in the study. The patients were given written and oral information about the study and were allowed to quit at any time. The patients arrived at the hospital at noon after having fasted since 6 o'clock the evening before. Forty-five minutes before the injection, the patients received 600 mL of oral purgative (Laxabon; BioPhausia). After intravenous administration of ^{18}F-FCH (administered activity, 4 MBq/kg of body weight—that is, between 280 and 430 MBq), subsequent PET images (thigh to neck) were acquired with a Philips Gemini TF PET/CT scanner at the following 4 time points: directly after the injection and at 1, 2, and between 3 and 4 h thereafter. The PET field of view was 18 cm with an overlap of 9 cm, with on average 9 bed positions per scan (2 min per bed position). Low-dose CT images (30 mAs; slice thickness, 5 mm; voxel size, 80 mm³) were obtained for attenuation and scatter correction immediately after injection and 2 and 3 h after injection. One hour after injection, 100 mL of intravenous x-ray contrast medium (Omnipaque 300 mg I/mL; GE Healthcare) were given to the patients, and a diagnostic CT image (120 mAs) was acquired. The patients were allowed to eat between the second and third acquisitions.

The activity concentrations in selected body organs and tissues, such as the liver, kidneys, spleen, urinary bladder, and, if present, tumor or metastases, were determined from the PET measurements using the software tool provided with the scanner (regions of interest manually defined). Then the concentrations were transformed into absolute activity values using the organ volumes determined from the registered CT images.

A specific correction was required for the measurements of the first scan in each patient. The first scan was indeed obtained immediately after injection, while the radiopharmaceutical was still being distributed to the organs and tissues. In this early phase, the result of the measurement can depend strongly on the position of the region of interest and on whether it was measured at the beginning or end of the scan. The software, however, refers the result of the measurement back to the beginning of the scan, correcting for the radioactive decay and neglecting the biokinetic variations during scan time. Therefore, significant systematic errors in the estimation of the initial activity concentration can occur. Because the accuracy of this information was of the uttermost importance for the correct development of the biokinetic model, an algorithm was implemented that identified the position of each organ and consequently the exact time point when that organ was imaged; retrieved the correct value of the measured activity concentration, cancelling the correction for radioactive decay introduced by the software; and referred the measured activity concentration to the exact time point of measurement (and not to the beginning of the scan).

The biokinetic variations during the later scans (at 1, 2, and between 3 and 4 h after injection) that differed from the first one were considered to be negligible, and no correction was performed.

Additionally, blood and urine samples were collected between the PET scans. Four to 5 blood samples were taken from the arm opposite the one used for injection. In 5 patients, the first sample was drawn within the first 2 min after administration, whereas in the other patients the first sample was drawn later, around 30 min after administration, because of operative problems. Four to 6 urine samples were collected for each patient at different time points after activity administration. Patients were asked to empty their bladder after the first scan. Additional urine samples were collected between scans, indicatively every hour, to obtain a detailed picture of the excretion pattern of ^{18}F. The concentration of ^{18}F in the biologic samples was measured in an automatic γ-counter (Wizard 1480; Wallac), introducing a correction for the counting efficiency at different activity levels. Total activity excreted in urine was calculated, multiplying the measured activity concentrations by the sample volumes, assessed by weighting.

Modeling

Evaluations for individual patients and population kinetic analysis were performed using 2 different software packages, SAAM II (13) and ADAPT 5 (14). For the population analysis, the maximum-likelihood approach using the expectation and maximization algorithm (15,16) was applied (MLEM approach). Identifiability of the compartment system (i.e., the possibility of having a finite or unique number of solutions for all of the model parameters) was verified using the GLOBI software (17).

Radiation Dosimetry

Radiation dose coefficients to the target regions r_T were calculated according to the formula:

$$d(r_T, T_D) = \sum_{r_S} \tilde{a}(r_S, T_D) S(r_T \leftarrow r_S), \qquad \text{Eq. 1}$$

where $\tilde{a}(r_S, T_D)$ is the time-integrated activity coefficient in source region r_S over dose-integration period T_D (i.e., the number of nuclear transformations in r_S after administration of an activity of 1 MBq to the patient) and $S(r_T \leftarrow r_S)$ is the mean absorbed dose rate to target region r_T per unit activity present in source region r_S (18).

Organ dose estimates were performed for a so-called reference patient and for each patient individually. In the first case, the time-integrated activity coefficients were evaluated using the biokinetic parameters derived from the population analysis, and the S factors of Equation 1 were derived using the adult male reference computational phantom (RCP-AM) recently adopted by the International Commission on Radiological Protection (ICRP) (19). For the individual dose estimates, the time-integrated activity coefficients were evaluated using the biokinetic parameters from the individual analysis. The S factors were based on the series of computational phantoms with different anatomic characteristics available at the Helmholtz Zentrum München (20). Additionally, 1 patient-specific voxel phantom was segmented from the CT data of 1 of the patients participating in this study (patient 1). The phantom was named MadPat (Madeira Patient).

Each single patient was individually associated to the phantom that most closely resembled his anatomic characteristics—that is, the phantom that minimized the following expression:

$$\Delta = \sqrt{\left(\frac{h_{pat} - h_{ph}}{h_{ph}}\right)^2 + \left(\frac{m_{pat} - m_{ph}}{m_{ph}}\right)^2}, \qquad \text{Eq. 2}$$

where h_{pat} and m_{pat} are the height and mass of the patient and h_{ph} and m_{ph} the corresponding quantities of the phantom. Table 1 summarizes the main features of the phantoms.

For each of the phantoms used, the S factors for ^{18}F were obtained, starting from specific absorbed fraction values for monoenergetic photons and electrons calculated with version V4-2-2-5 of the EGSnrc Monte Carlo code package (21) using the nuclear decay data from ICRP publication 107 (22).

TABLE 1
Physical Characteristics of Computational Phantoms

Characteristic	Phantom name			
	RCP-AM	Frank	MadPat	Visible Human
Age (y)	NA	48	69	38
Height (cm)	176	174	172	180
Weight (kg)	73	95	70	103
No. of voxels (millions)	1.95	23.7	8.3	20.1
Slice thickness (mm)	8	5	5	5
Voxel volume (mm^3)	36.5	2.7	6.9	4.3
Coverage	Whole body	Head and trunk	Head to thigh	Head to thigh

To evaluate the whole-body exposure of the prostate cancer reference patient undergoing an ^{18}F-FCH study, a quantity was calculated, which we refer to as the risk-weighted absorbed dose coefficient defined following the quantity effective dose in ICRP publication 60 (23):

$$e = \sum_T w_T \; d(r_T, T_D), \qquad \text{Eq. 3}$$

where the list of target organs r_T, composition of the remainder, and values of the weighting factors w_T are those presented in ICRP publication 60.

RESULTS

Biokinetic Data

Figure 1 shows that the biokinetic patterns are similar in all individuals. The concentration in blood decreases rapidly in the first hour after administration. The greatest interindividual variations were observed for the concentration values in the first collected blood sample. For the liver, kidney, and spleen, the activity curves (not corrected for radioactive decay) reach their maxima in the first scan. Indicative maximum values correspond to about 11% of the injected activity for the liver, 5% for the kidneys, and 1% for the spleen. Activity for the liver and the spleen decreases with half-times similar to the physical half-time of ^{18}F, the decrease for the kidneys is faster. Urinary excretion is rapid; most of the activity is eliminated in the first hour after administration.

Model Development

The starting model structure featured a central exchange compartment (blood) in which the injected radiopharmaceutical was initially distributed and a series of subsystems representing the organs and tissues in which most of the activity was concentrated and that were imaged in all patients: liver, kidneys, spleen, and urinary bladder. A further compartment (rest of the body [RoB]) was added to account for the material transported to organs and tissues different from those explicitly modeled. For some patients, activity concentrations were available also for the salivary glands, tumors, or metastatic tissues. The activities present in these regions were, however, small; thus, it was decided not to indicate them explicitly in the model structure and include them in the RoB.

The first tests showed that such a simple model structure was unable to describe simultaneously and with sufficient realism the available experimental data. Two strategies were pursued to refine the model structure. On the one hand, the possibility of using nonlinear kinetics for some transfer processes was investigated (11). As an alternative, the so-called forcing-function approach (24) was used here: the original simple model structure was split into several independent subsystems. The decoupling was achieved using a sum of exponentials with fixed coefficients (the forcing function) to describe the activity in the central compartment (blood). The forcing function was then applied as an input for each peripheral compartment separately, and the best structure and the parameter values for each subsystem were determined, fitting the model predictions only to the data collected in that subsystem. The separate substructures were then recombined into the complete model, the forcing function lifted, and the new fit performed in the recombined structure, using as starting estimates the parameter values obtained in the previous analysis.

The final structure of the model is shown in Figure 2. The compartment liver had to be split into 2 subunits, the first one exchanging material with blood and the second one eliminating it through the biliary-fecal pathway. Two compartments were used to describe the kidneys as well, adopting the representation commonly used by the ICRP: urinary excretion is assumed to arise from direct transfer to the urinary bladder and from delayed transfer after retention in the kidney tissues (urinary path).

Table 2 reports the values of the model parameters estimated with the population analysis and the ranges of the model parameter values estimated with the individual analysis. Figure 1 compares the population model predictions of the activity in blood, liver, kidneys, and spleen, and of the urinary excretion rate with the corresponding sets of data. For a better comparison with the available data, the model prediction of the average urinary excretion rate is expressed as a step function over consecutive collection periods of 1 h. Supplemental Figure 1 (supplemental materials are available online only at http://jnm.snmjournals.org) compares the individual model predictions of the activity in the liver, kidneys, and blood for each patient with that patient's corresponding data.
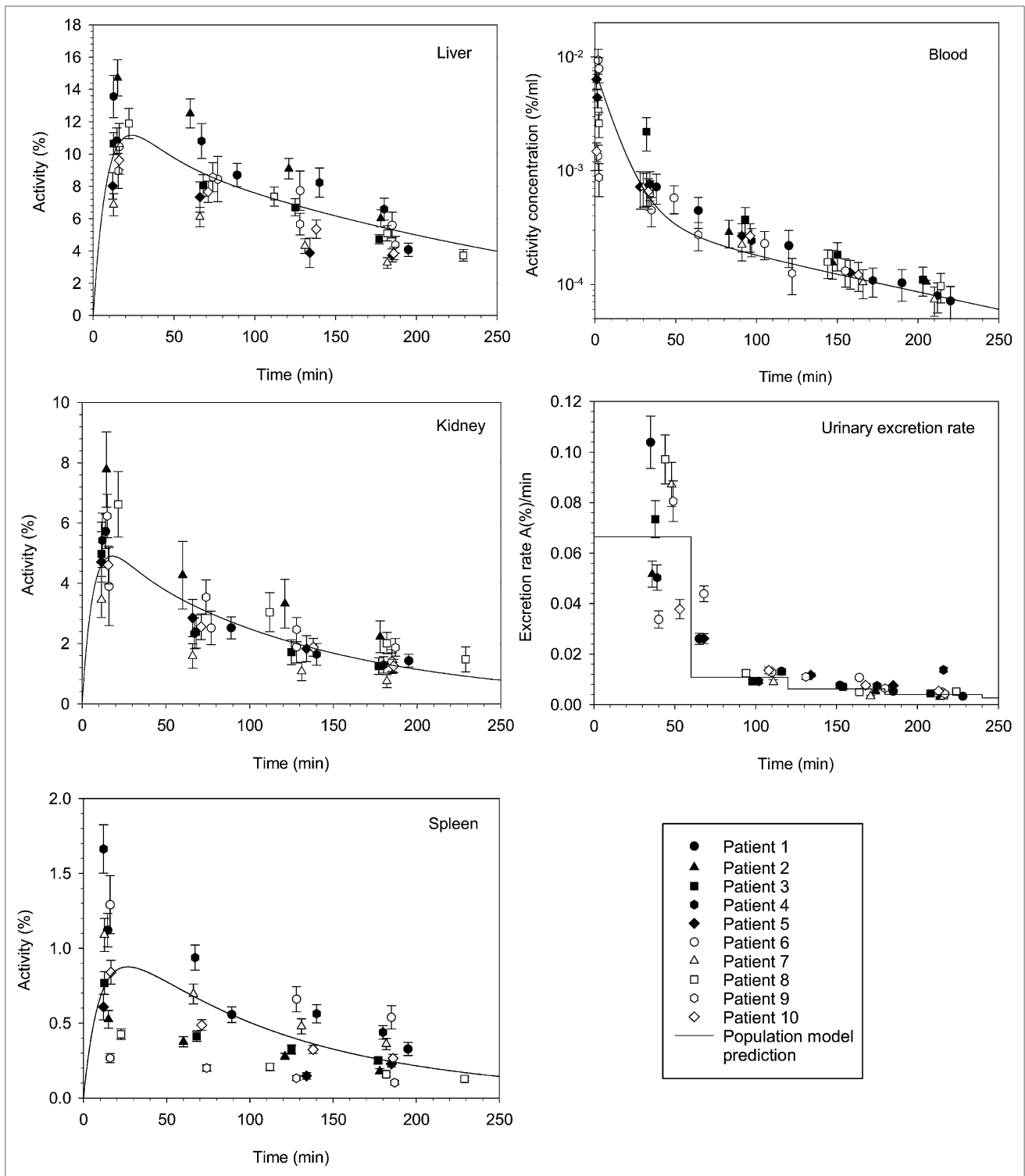
FIGURE 1. Biokinetic data measured in 10 patients. Uncertainty bars in liver, kidneys, and spleen correspond to 1 SD and combine statistical uncertainty provided by software that calculates activity concentration in region of interest and uncertainty on organ volume from registered CT scan. Uncertainty bars in urine and blood data correspond to 1 SD from measurements of duplicate specimen of same sample. Solid lines represent results of population analysis with compartmental structure of Figure 2.

Dosimetry

Table 3 shows the time-integrated activity coefficients for the reference patient calculated using the results of the population analysis. Also, the maximum, minimum, mean, and median values of the coefficients calculated for each of the 10 patients (individual analysis) are shown. For calculating the activity coefficients in the urinary bladder, 2 assumptions were made: bladder voiding every hour, in
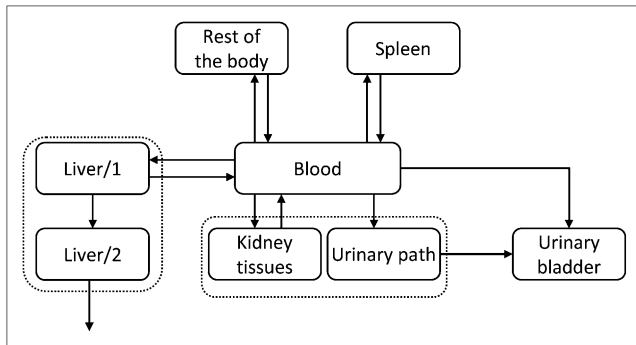
FIGURE 2. Proposed structure of compartmental model for biokinetics of ^{18}F-FCH.

accordance with the collection schedule followed by the patients, and bladder voiding every 3.5 h, as generally assumed in the ICRP calculations.

These values were used as an input for the calculation of the organ doses received during an ^{18}F-choline study. Table 4 reports the results for the reference patient. The doses were calculated using the S values obtained with the adult male reference computational phantom (RCP-AM) recently adopted by ICRP (*19*). For comparison, the table also shows the dose values calculated with the software OLINDA/EXM (*25*), which uses the conventional S values obtained with a set of stylized mathematic phantoms (*26*).

The risk-weighted absorbed dose coefficient for the reference patient, calculated according to Equation 3 using the organ dose coefficients given in the "RCP-AM" columns of Table 4, amounts to 0.018 mSv/MBq in the case of the bladder-voiding interval of 1 h. Considering bladder voiding every 3.5 h has only a limited effect on the coefficient (0.019 mSv/MBq).

The individual organ doses were calculated for each patient using the appropriate voxel phantom identified by the simple algorithm described by Equation 2. The following

associations were found: patients 1 and 2, MadPat; patients 3, 8, and 9: RCP-AM; patients 4 and 7, Frank; and patients 5, 6, and 9, Visible Human.

The ranges (maximum, minimum, mean, and median values) of the individual doses to selected target organs are summarized in Table 5 and compared with the values obtained for the reference patient.

DISCUSSION

Figure 1 and Supplemental Figure 1 show that the model is successful in describing the average behavior of the measured data and can be easily characterized for each individual patient. The greatest deviations are observed in the description of the initial blood clearance, for which the spread of the data is higher.

The parameter values obtained from the population analysis (reference patient) indicate that ^{18}F-choline is eliminated rapidly from blood and that the biologic clearance time equals 7.5 min. Amount of material transported to liver is 17.4%, to the kidney tissues 5.2%, to the spleen 1.2%, and to the compartment RoB 71.1%. The remaining 5.1% is excreted into the urine, mostly through the urinary path. The transit time in the urinary path is 7.15 min.

In our model, the liver is split into 2 compartments: Liver1 describes the exchange with blood, and Liver2 describes long-time retention and excretion through the biliary pathway. The half-time of the exchange process is approximately 17 min. Slightly less than the half (44%) of the material present in the liver goes back to blood; the remaining 56% proceeds toward the biliary excretion pattern. Because of the short physical half-life of ^{18}F and the duration of the studies, it was not possible to determine the long-term retention component in the compartment Liver2.

The compartments spleen, kidney tissues, and RoB recycle choline back to blood with biologic half-times of 90, 110, and 150 min, respectively.

TABLE 2
Values of Model Parameters (min^{-1}) as Obtained from Fits

Parameter	Population analysis			Individual analysis		
	Mean	Population SD	Coefficient of variation (%)	Median	Minimum	Maximum
Blood to liver1	1.61×10^{-2}	0.32×10^{-2}	20	1.63×10^{-2}	1.08×10^{-2}	2.18×10^{-2}
Liver1 to blood	1.84×10^{-2}	0.40×10^{-2}	22	1.87×10^{-2}	1.33×10^{-2}	2.61×10^{-2}
Liver1 to liver2	2.3×10^{-2}	1.7×10^{-2}	74	1.72×10^{-2}	9.00×10^{-3}	6.27×10^{-2}
Blood to spleen	1.13×10^{-3}	0.51×10^{-3}	45	1.03×10^{-3}	3.63×10^{-4}	1.98×10^{-3}
Spleen to blood	7.7×10^{-3}	2.6×10^{-3}	34	7.04×10^{-3}	3.78×10^{-3}	1.26×10^{-2}
Blood to urinary bladder	5.1×10^{-4}	3.0×10^{-4}	59	5.40×10^{-4}	1.84×10^{-4}	9.56×10^{-4}
Blood to kidney tissues	4.8×10^{-3}	1.3×10^{-3}	27	4.51×10^{-3}	2.97×10^{-3}	6.62×10^{-3}
Kidney tissues to blood	6.2×10^{-3}	3.2×10^{-3}	52	5.21×10^{-3}	2.50×10^{-3}	1.11×10^{-2}
Blood to urinary path	4.2×10^{-3}	1.1×10^{-3}	26	4.16×10^{-3}	2.47×10^{-3}	5.94×10^{-3}
Urinary path to bladder	9.7×10^{-2}	2.9×10^{-2}	30	9.68×10^{-2}	4.46×10^{-2}	1.25×10^{-1}
Blood to RoB	6.56×10^{-2}	0.91×10^{-2}	14	6.56×10^{-2}	5.46×10^{-2}	8.32×10^{-2}
RoB to blood	4.6×10^{-3}	2.4×10^{-3}	52	3.98×10^{-3}	1.44×10^{-3}	8.92×10^{-3}
Blood volume	1.28×10^{4}	0.83×10^{4}	65	9.39×10^{3}	3.45×10^{3}	2.51×10^{4}

TABLE 3
Time-Integrated Activity Coefficients (Hours)

Source organ	Reference patient	Individual analysis			
		Minimum	Maximum	Mean	Median
Liver	0.422	0.293	0.489	0.388	0.388
Kidneys	0.114	0.067	0.163	0.119	0.113
Spleen	0.022	0.008	0.034	0.022	0.021
Urinary bladder contents*	0.039	0.026	0.052	0.039	0.040
Urinary bladder contents†	0.119	0.080	0.156	0.117	0.122
Blood	0.270	0.196	0.421	0.280	0.251
Rest of body	1.621	1.503	1.866	1.643	1.614

*Bladder-voiding interval, 1 h.
†Bladder-voiding interval, 3.5 h.

One reason for using population analysis was that this analysis can account separately for within- and between-individual sources of variability, thus distinguishing between the uncertainty sources that are due to the measurements or to the inability of the model to describe the data (it should be always considered that the mathematic models used are a rough approximation of the actual biologic processes going on) and those that are due to interindividual variability (the population SD indicated in the table). The range of variability of the individual estimates is also indicated as a further term of comparison.

The population SD of the model parameters is in most cases limited to 35% or less of the parameter value, and only 2 parameters have coefficients of variation greater than 60%. The parameters with the highest relative SD are those describing the longer-term processes, such as feedback to blood from the organs or transfer to biliary excretion. One explanation is that the physical half-life of ^{18}F is too short to enable the observation of such processes as long as required for accurate parameter determination. These parameters are indeed the ones showing also the highest interindividual variations. Furthermore, the value of the blood volume (distribution compartment) has a relatively high population SD and large interindividual variability. The estimates, ranging from 3.45 to 25.1 L, suggest that ^{18}F-FCH may be initially distributed also in the interstitial fluids. This parameter was difficult to estimate with sufficient precision, because for several patients the first sample was collected only after more than 30 min. Additionally, for the patients who provided a blood sample immediately after

TABLE 4
Committed Organ Dose Coefficients for Reference Patient (mGy/MBq)

Organ	Bladder-voiding interval			
	1 h		3.5 h	
	RCP-AM	OLINDA/EXM	RCP-AM	OLINDA/EXM
Kidneys	0.079	0.078	0.079	0.078
Liver	0.062	0.056	0.062	0.056
Spleen	0.038	0.030	0.038	0.030
Adrenals	0.027	0.017	0.027	0.017
Pancreas	0.022	0.016	0.022	0.016
Lung	0.018	0.011	0.018	0.011
Stomach wall	0.018	0.013	0.018	0.013
Esophagus wall	0.018	—	0.018	—
Urinary bladder wall	0.017	0.029	0.030	0.066
Colon wall	0.014	0.013	0.015	0.013
Small intestine wall	0.014	0.013	0.015	0.013
Thymus	0.013	0.010	0.013	0.010
Bone marrow	0.012	0.010	0.013	0.010
Breast	0.011	0.0085	0.011	0.0085
Thyroid	0.011	0.0095	0.011	0.0095
Muscle	0.0095	0.010	0.0097	0.010
Bone surface	0.0094	0.015	0.0097	0.015
Gonads	0.0093	0.0093	0.0096	0.010
Brain	0.0078	0.0082	0.0078	0.0082
Skin	0.0074	0.0078	0.0075	0.0079

TABLE 5
Committed Organ Dose Coefficients (mGy/MBq)

Target region	Individual				Reference patient
	Minimum	Maximum	Mean	Median	
Liver	0.036	0.082	0.054	0.053	0.062
Kidneys	0.033	0.105	0.066	0.067	0.079
Spleen	0.014	0.040	0.027	0.027	0.038
Urinary bladder wall	0.015	0.037	0.022	0.020	0.017
Other tissues	≤0.022	≤0.032	—	—	≤0.031

injection, the measured concentrations show large interindividual variations. In this case, even small uncertainties in the determination of the time of blood withdrawal (which are unavoidable in a complex study involving suffering patients) might affect significantly the parameter estimation process, because of the extreme rate of the initial clearance.

As already explained, previous studies had collected information on the biodistribution of choline only up to about 1 h after administration. DeGrado et al. (4) acquired whole-body PET images for male and female patients starting 10–20 min after ^{18}F-FCH administration. They found lower mean uptake values in liver (~14%) and higher ones in kidneys (between 8.2% and 9.1%) and spleen (between 1.3% and 3.0%) than in the present study. The high values for kidneys and spleen observed there should, however, be considered with caution, because a closer look at Table 3 of that work suggests that the uptakes have been estimated using rather large values of the organ masses. Similarly, Schmid et al. (6) indicated kidneys, liver, spleen, and also pancreas as preferred sites of ^{18}F-FCH localization.

DeGrado et al. (4), using dynamic PET of the cardiac blood pool, observed a rapid phase of blood clearance (nearly complete after 3 min). The experimental schedule used in the present study did not allow for verification of this feature; however, the large differences observed in the initial blood concentration values partially confirm it.

Choline can be administered also labeled with [11]C. There is experimental evidence of potential differences between the pharmacokinetics of ^{18}F-choline and ^{11}C-choline, especially with regard to the excretion pathways (^{11}C-choline is not excreted in the urine). As discussed by DeGrado et al. (4), these differences may be attributed to the presence of the fluorine atom, which renders the choline molecule less susceptible for oxidation to betaine, as usually observed with ^{11}C-choline (3). The model presented here might, therefore, not be applicable to the biokinetics of ^{11}C-choline.

The dose estimates given in Table 4 show that the most exposed organs are those that could be easily imaged in the PET study and, therefore, explicitly introduced in the model structure (kidneys, liver, spleen). Comparable doses were calculated for adrenals, pancreas, and organs of the alimentary tract. The dose to the urinary bladder increases by about a factor of 2 (0.030 vs. 0.017 mGy/MBq) when the bladder-voiding interval of 3.5 h is used instead of 1 h.

Nonnegligible differences between the dosimetric estimates obtained with the RCP-AM phantom and the conventional ones obtained with the OLINDA/EXM software can be observed for several organs, although both calculations start from the same values of time-integrated activity coefficients presented in Table 3. In particular, the doses calculated with the adult male reference computational phantom are higher for nearly all target regions, with the noteworthy exception of the urinary bladder wall and of the bone surface. The observed differences are ascribable partially to the greater realism of the new computational phantoms in terms of organ shape and position and partially to the different assumptions used in the description of the radiation transport processes. The specific absorbed fraction values obtained with the RCP-AM phantom include explicit Monte Carlo calculation of the electron absorption. In OLINDA/EXM corrections for electron escape are performed for small organs and high energies on the basis of self-absorption specific-absorbed fractions for unit-density spheres, but electron cross-fire to neighboring organs is not considered (25,27).

These different assumptions affect particularly the calculation of energy deposition for radionuclides contained inside a walled organ, such as urinary bladder, and emitting nonpenetrating β-radiation. Significant differences especially for electron energies below 1 MeV can be expected.

With regard to the intraindividual variability, it can be observed from Table 5 that the spread of dose coefficients between single patients is relatively limited, the ratio maximum value to minimum value being between 2.2 and 3.2. This spread takes into account differences in the biokinetics and in anatomy, because different phantoms were used for the different patients.

The fact that the kidneys represent the dose-critical organ is in agreement with the dose estimates previously available (4,28), but the dose values obtained in this study are generally lower than the previous estimates.

DeGrado et al. (4) performed dosimetric calculations on the basis of their biodistribution data, assuming immediate uptake in the organ, infinite retention, and no elimination from the bladder. For male patients, they found organ doses of 0.159, 0.063, 0.059, and 0.054 mGy/MBq for the kidneys, urinary bladder wall, liver, and spleen, respectively.

Based on the same data, Noßke and Brix (*28*) performed dosimetric calculations with OLINDA/EXM, assuming organ uptake values of 14%, 9%, and 2% for the liver, kidneys, and spleen, respectively. They considered infinite retention time in the organs and a bladder-voiding interval of 3.5 h. Using these conservative assumptions, they found organ doses of 0.150, 0.063, 0.051, and 0.047 mGy/MBq for the kidneys, spleen, liver, and urinary bladder wall, respectively.

The doses for kidneys and spleen calculated by DeGrado et al. (*4*) and by Noßke and Brix (*28*) are higher than those obtained in this work using the conventional approach. Doses for the liver and urinary bladder are comparable to or slightly lower than the ones reported here. The assumption of infinite retention time in the organs tends indeed to overestimate the number of disintegrations in the organs and to underestimate the ones in the urinary bladder. For liver, the overestimation due to the assumption of infinite retention is compensated by the lower liver uptake found by DeGrado et al. The estimates of DeGrado et al. and those of Noßke and Brix fall outside the range of variability of the individual doses observed in this study for the kidneys, spleen, and urinary bladder wall. For the urinary bladder wall, the different assumptions used for describing bladder emptying and the more realistic description of electron transport in walled organs obtainable with the computational phantoms should be considered.

The effective dose, as defined by ICRP in publication 60 (*23*), is the quantity commonly reported as a generic index of risk, and it is used for prospective radiologic protection of a population of both sexes. Hence, it should not be used as an index of stochastic risk to a single individual patient, nor can it be assigned to male or female patients of body morphometries significantly different from those of the ICRP reference individuals (*19*). Furthermore, according to the new recommendations of the ICRP (*29*), which have superseded publication 60, the calculation of effective dose requires averaging organ doses assessed separately for male and female reference individuals and then weighting by sex- and age-averaged factors. The group of patients investigated in this work is exclusively male and cannot be considered representative of the reference individual for which the effective dose is calculated. Therefore, the quantity risk-weighted absorbed dose coefficient was introduced for the whole-body exposure of the reference patient undergoing an ^{18}F-FCH study. In this way, it was possible to evaluate a quantity that can be easily compared with literature values of effective dose. The value of 0.018 mSv/MBq obtained for the risk-weighted absorbed dose coefficient is comparable to the effective dose coefficient of 0.017 mSv/MBq evaluated by Noßke and Brix (*28*).

CONCLUSION

A compartmental model structure for describing the biokinetics and dosimetry of ^{18}F-FCH in prostate cancer patients was developed. The model proved to give a satisfactory description of the biodistribution of ^{18}F-FCH and realistic estimates of the radiation dose received by the patients. Interindividual variations of the model parameters were significant only for those long-term model features that could not be accurately investigated because of the physical half-life of ^{18}F. The range of variability of the individual organ doses was in the worst case about a factor 3.

The model structure can furthermore be refined to take into account uptake and retention in malignant or metastatic regions and thus be used as a starting point for the optimization of the imaging protocol.

DISCLOSURE STATEMENT

ACKNOWLEDGMENTS

REFERENCES

1. Ackerstaff E, Glunde K, Bhujwalla Z. Choline phospholipid metabolism: a target in cancer cells? *J Cell Biochem.* 2003;90:525–533.
2. Ramírez de Molina A, Rodriguez-Gonzalez A, Gutierrez R, Martinez-Pineiro L, Sanchez J, Bonilla F. Overexpression of choline kinase is a frequent feature in human tumor-derived cell lines and in lung, prostate, and colorectal human cancers. *Biochem Biophys Res Commun.* 2002;296:580–583.
3. Kwee SA, Wei H, Sesterhenn I, Yun D, Coel MN. Localization of primary prostate cancer with dual-phase ^{18}F-fluorocholine PET. *J Nucl Med.* 2006;47:262–269.
4. DeGrado TR, Reiman RE, Price DT, Shuyan W, Coleman RE. Pharmacokinetics and radiation dosimetry of ^{18}F-fluorocholine. *J Nucl Med.* 2002;43:92–96.
5. Sutinen E, Nurmi M, Roivainen A, et al. Kinetics of [^{11}C]choline uptake in prostate cancer: a PET study. *Eur J Nucl Med Mol Imaging.* 2004;31:317–324.
6. Schmid DT, John H, Zweifel R, et al. Fluorocholine PET/CT in patients with prostate cancer: initial experience. *Radiology.* 2005;235:623–628.
7. Steiner C, Vees H, Zaidi H, et al. Three-phase ^{18}F-fluorocholine PET/CT in the evaluation of prostate cancer recurrence. *Nuklearmedizin.* 2009;48:1–9.
8. Uusijärvi H, Nilsson LE, Bjartell A, Mattsson S. Biokinetics of ^{18}F-choline studied in four prostate cancer patients. *Radiat Prot Dosimetry.* 2010;139:240–244.
9. Hoeschen C, Mattsson S, Cantone MC, et al. Minimising activity and dose with enhanced image quality by radiopharmaceutical administrations. *Radiat Prot Dosimetry.* 2010;139:250–253.
10. Roivainen A, Forsback S, Grönroos T, et al. Blood metabolism of [methyl-^{11}C]choline; implications for in vivo imaging with positron emission tomography. *Eur J Nucl Med.* 2000;27:25–32.
11. Tavola F, Janzen T, Giussani A, et al. Non-linear compartmental model of ^{18}F-choline. *Nucl Med Biol.* 2012;39:261–268.
12. Janzen T, Tavola F, Giussani A, et al. Compartmental model of ^{18}F-choline. In: Molthen RC, Weaver JB, eds. *Medical Imaging 2010: Biomedical Applications in Molecular, Structural, and Functional Imaging.* Bellingham, WA: SPIE; 2010.

13. Barrett PHR, Bell BM, Cobelli C, Golde H, Schumitzky A, Vicini P. SAAM II: simulation, analysis, and modeling software for tracer and pharmacokinetic studies. *Metabolism.* 1998;47:484–492.

14. D'Argenio DZ, Schumitzky A, Wang X. *ADAPT 5 User's Guide: Pharmacokinetic/Pharmacodynamic Systems Analysis Software.* Los Angeles, California: Biomedical Simulations Resource; 2009.

15. Dempster AP, Laird NM, Rubin DB. Maximum likelihood from incomplete data via the EM algorithm. *J R Stat Soc, B.* 1977;39:1–38.

16. Walker S. An EM algorithm for nonlinear random effects models. *Biometrics.* 1996;52:934–944.

17. Audoly S, D'Angio L, Saccomanni MP, Cobelli C. Global identifiability of linear compartment models: a computer algebra algorithm. *IEEE Trans Biomed Eng.* 1998;45:36–47.

18. Bolch WE, Eckerman KF, Sgouros G, Thomas SR. MIRD pamphlet no. 21: a generalised schema for radiopharmaceutical dosimetry: standardization of nomenclature. *J Nucl Med.* 2009;50:477–484.

19. International Commission on Radiological Protection (ICRP). ICRP publication 110: adult reference computational phantoms. *Ann ICRP.* 2009;39.

20. Petoussi-Henss N, Zankl M, Fill U, Regulla D. The GSF family of voxel phantoms. *Phys Med Biol.* 2002;47:89–106.

21. Kawrakow I, Rogers DWO. *The EGSnrc Code System: Monte Carlo Simulation of Electron and Photon Transport.* PIRS report 701, 4th ed. Ottawa, Canada: National Research Council of Canada; 2003.

22. International Commission on Radiological Protection (ICRP). ICRP publication 107: nuclear decay data for dosimetric calculations. *Ann ICRP.* 2008;38.

23. International Commission on Radiological Protection (ICRP). ICRP publication 60: 1990 recommendations of the International Commission on Radiological Protection. *Ann ICRP.* 1991;21.

24. Foster DM. Developing and testing integrated multicompartment models to describe a single-input multiple-output study using the SAAM II software system. In: Clifford AJ, Müller H-G, eds. *Mathematical Modeling in Experimental Nutrition.* New York, NY: Plenum Press; 1998: 59–78.

25. Stabin MG, Sparks RB, Crowe E. OLINDA/EXM: the second-generation personal computer software for internal dose assessment in nuclear medicine. *J Nucl Med.* 2005;46:1023–1027.

26. Cristy M, Eckerman KF. *Specific Absorbed Fractions of Energy at Various Ages from Internal Photon Sources. I. Methods.* Report ORNL/TM-8381/V1. Oak Ridge, TN: Oak Ridge National Laboratory; 1987.

27. Stabin MG, Kroijnenberg M. Re-evaluation of absorbed fractions for photons and electrons in small spheres. *J Nucl Med.* 2000;41:149–160.

28. Noßke D, Brix G. Dose assessment for C-11 and F-18-choline [abstract]. *J Nucl Med.* 2009;50(suppl 2):1851P.

29. International Commission on Radiological Protection (ICRP). ICRP publication 103: the 2007 recommendations of the International Commission on Radiological Protection. *Ann ICRP.* 2007;37.